nature cell biology

The Cdk1–APC/C cell cycle oscillator circuit functions as a time-delayed, ultrasensitive switch

Qiong Yang[1] and James E. Ferrell Jr[1,2,3]

Despite the complexity and variety of biological oscillators, their core design invariably includes an essential negative feedback loop. In the *Xenopus laevis* embryonic cell cycle oscillator, this loop consists of the kinase cyclin B–Cdk1 and the ubiquitin ligase APC/C^{Cdc20}; active Cdk1 activates APC/C^{Cdc20}, which then brings about cyclin B degradation and inactivates Cdk1. Here we ask how this negative feedback loop functions quantitatively, with the aim of understanding what mechanisms keep the Cdk1–APC/C^{Cdc20} system from settling into a stable steady state with intermediate levels of Cdk1 and APC/C^{Cdc20} activity. We found that the system operates as a time-delayed, digital switch, with a time lag of ∼15 min between Cdk1 and APC/C^{Cdc20} activation and a tremendously high degree of ultrasensitivity ($n_H \approx 17$). Computational modelling shows how these attributes contribute to the generation of robust, clock-like oscillations. Principles uncovered here may also apply to other activator–repressor oscillators and help in designing robust synthetic clocks.

Organisms from cyanobacteria to vertebrates make use of biochemical oscillators to drive repetitive processes such as cell cycle progression and vertebrate somitogenesis. Oscillators also enable organisms to anticipate natural environmental rhythms, as exemplified by the circadian clock. The timescales of biological oscillations vary widely (over more than ten orders of magnitude[1]) and the components of oscillator circuits are highly diverse. Nevertheless, it is thought that all biological oscillators share certain common design principles.

For example, oscillators generally depend on negative feedback[2]. However, absent crucial elements, negative feedback circuits often settle into a stable steady state rather than oscillating[3]. Computational studies have enumerated several modifications of the basic activator–repressor circuit that can promote oscillations[1,4–8]. These include time delays, which can be generated by the addition of intermediary species to the negative feedback loop; ultrasensitivity in the steady-state responses of the loop's components to their upstream regulators; and interlinked positive feedback loops, which can serve as a bistable trigger. This raises the question of which of these strategies are actually used in the complex biological oscillator circuits found in nature.

Here we focus on the *Xenopus laevis* embryonic cell cycle, which is driven by an autonomous biochemical oscillator[9,10]. The core of the oscillator is a negative feedback loop that includes the Cdk1–cyclin B protein kinase and the E3 ubiquitin ligase APC/C^{Cdc20}. Active Cdk1–cyclin B brings about activation of APC/C^{Cdc20} through an incompletely understood mechanism[11]. In turn, active APC/C^{Cdc20} polyubiquitylates the mitotic cyclins, tagging them for degradation by the proteasome[12] and completing the loop.

The Cdk1 system also includes interlinked positive and double-negative feedback loops, involving the protein kinases Wee1A and Myt1 and the phosphatases Cdc25A and Cdc25C, which collectively function as a bistable trigger[13,14]. Compromising the bistable trigger suppresses oscillations in *Xenopus* egg extracts[15], indicating that positive feedback can promotes oscillations. Here we examine the quantitative properties of the core negative feedback itself, with the aim of understanding how this loop contributes to the robust, autonomous oscillations seen in the early embryo.

We first examined how the steady-state rate of degradation of securin–CFP (a substrate of APC/C^{Cdc20}; CFP, cyan fluorescent protein) varies with the activity of Cdk1, because ultrasensitivity in this response could promote oscillations. We made use of cycloheximide-treated interphase *Xenopus* egg extracts for these studies. We added various concentrations of non-degradable Δ65-cyclin B1 to the extracts in the presence of PD0166285, an inhibitor of Wee1A and Myt1 that effectively neutralizes the positive feedback loops of the mitotic trigger and enables intermediate levels of Cdk1 activity to be obtained (Fig. 1a–c). Securin–CFP was then added, and the time course of its degradation was monitored with a fluorescence plate reader. Securin–CFP fluorescence decreased exponentially with time in extracts treated with mitotic concentrations of Δ65-cyclin B1 (Fig. 1d). Similar

[1]Department of Chemical and Systems Biology, Stanford University School of Medicine, Stanford, California 94305-5174, USA. [2]Department of Biochemistry, Stanford University School of Medicine, Stanford, California 94305-5174, USA.
[3]Correspondence should be addressed to J.E.F. (e-mail: james.ferrell@stanford.edu)

Received 7 September 2012; accepted 18 March 2013; published online 28 April 2013; DOI: 10.1038/ncb2737

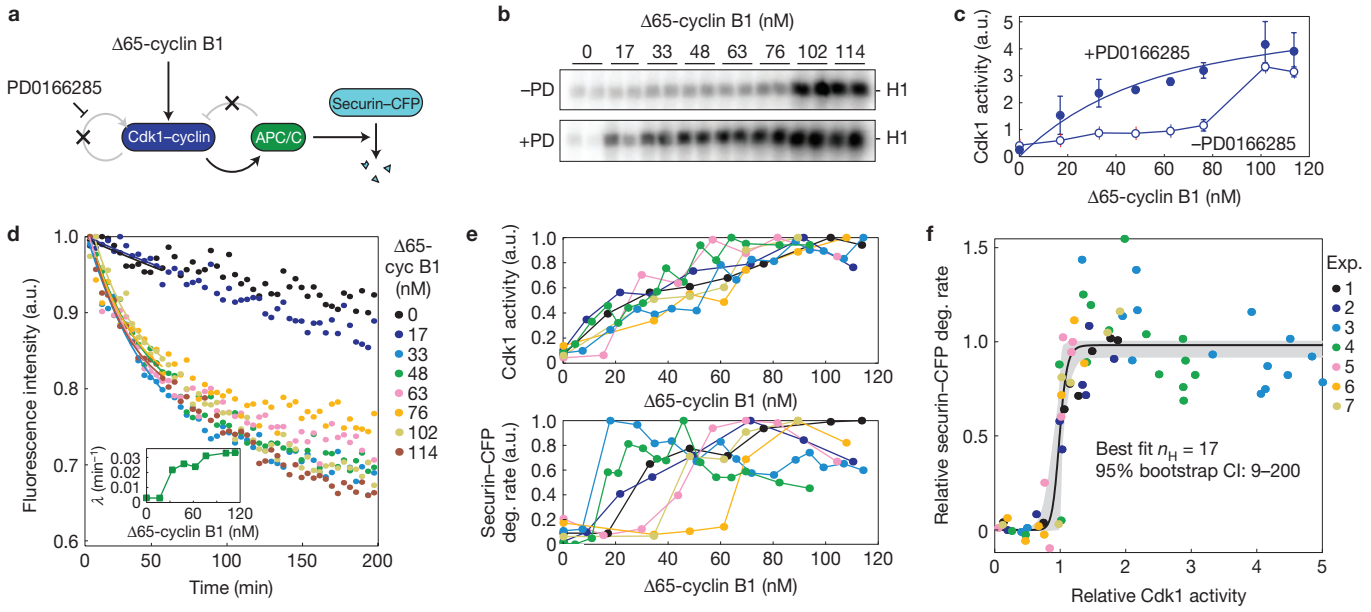

Figure 1 Ultrasensitivity in the regulation of securin–CFP destruction by Cdk1. (**a**) Schematic depiction of the experimental approach. (**b**,**c**) The response of Cdk1 to Δ65-cyclin B1 (monitored as phosphorylation of histone H1) is all-or-none in the absence of PD0166285 (**b**) and graded in its presence (500 nM; **c**). (**d**) Degradation of securin–CFP in extracts. Extracts were treated with eight concentrations of Δ65-cyclin B1 (shown in different colours) for 90 min to enable Cdk1 and APC/C^{Cdc20} activities to reach steady state. *In vitro*-translated securin–CFP was then added and the securin–CFP fluorescence was monitored in a plate reader. The inset shows the apparent first-order rate constant λ as a function of the Δ65-cyclin B1 concentration. Addition of the MEK inhibitor U0126 to the extracts had little apparent effect on securin–CFP degradation, suggesting that there is too little Mos left in these extracts to exert measurable cytostatic factor activity (Supplementary Fig. S1). (**e**) Cdk1 activity (top) and securin–CFP degradation (deg.; bottom) as a function of the Δ65-cyclin B1 concentration. Data are from seven independent experiments, with each experiment designated by a different colour. (**f**) Pooled data on securin–CFP degradation versus Cdk1 activity. Data are from seven independent experiments and are scaled relative to the individual experiments' maximum degradation rates and EC_{50} values. CI, confidence interval. See also Supplementary Fig. S1.

results were obtained in the presence of the MAP-kinase kinase (MEK) inhibitor U0126 (Supplementary Fig. S1), suggesting that any residual Mos is too low in concentration to exert a significant cytostatic factor effect.

As shown in Fig. 1d, securin–CFP degradation was a switch-like function of the Cdk1 activity. The degradation rate was low in extracts treated with 0 or 17 nM Δ65-cyclin B1, and near maximal in extracts treated with 33 nM Δ65-cyclin B1. These results fit well with earlier studies[16], and extend those studies by showing that, even when Cdk1 activation is forced to be graded, the degradation of this APC/C^{Cdc20} substrate is still highly ultrasensitive.

This experiment was repeated, and in all cases the Cdk1 response was graded and the securin–CFP degradation response was switch-like, although the half-maximum effective concentration (EC_{50}) values for both responses varied substantially from experiment to experiment (Fig. 1e; see also Supplementary Information). Similarly high variability was found for the responses of two other Cdk1 substrates studied previously, Wee1A (ref. 17) and Cdc25C (ref. 18), possibly because of varying amounts of phosphatase activity in different extracts[19]. Whatever the source of variability, we found that the APC/C^{Cdc20} responses were ultrasensitive regardless of whether a high or low concentration of cyclin was required for APC/C^{Cdc20} activation (Fig. 1).

To quantify the nonlinearity from all experiments, the data were scaled, pooled and fitted to a single Hill function. The fitted Hill exponent n_H was 17, with a 95% bootstrap confidence interval of 9–200 (Fig. 1f). Therefore, securin–CFP degradation is essentially digital, switching from maximally off to maximally on over a tight range of Cdk1 activities. Similar results were obtained for the degradation of *in vitro*-translated cyclin B1–CFP, added at concentrations too low to yield significant Cdk1 activity (Fig. 2a,b).

We also examined the degradation of cyclin A2, which interacts differently with APC/C^{Cdc20} than cyclin B1 does[20], and hence could exhibit a qualitatively different stimulus–response relationship. To enable a direct comparison, we carried out two-colour fluorescence studies using *in vitro*-translated securin–CFP and cyclin A2–YFP (yellow fluorescent protein). As shown in Fig. 2c–e, cyclin A2–YFP was degraded more rapidly than securin–CFP, which could explain the observation that in *Xenopus* extracts, where the spindle assembly checkpoint is not operative[21], cyclin B1 destruction still lags behind cyclin A2 destruction[22]. The two substrates exhibited similarly switch-like dose–response curves, suggesting that ultrasensitivity is a general feature of the degradation of APC/C^{Cdc20} targets.

Note that *Saccharomyces cerevisiae* APC/C^{Cdc20} has been reported to undergo intramolecular ubiquitylation of its Cdc20 subunit, resulting in destruction of Cdc20 and auto-inactivation of the complex[23]. If this is true of *Xenopus* APC/C^{Cdc20}, then both the auto-inactivation rate constant and the securin–CFP destruction rate constant would factor into the apparent first-order rate constant for securin–CFP destruction. However, no obvious decreases were seen in APC/C^{Cdc20} activity in *Xenopus* extracts over at least the first hour of incubation. For these reasons we infer that APC/C^{Cdc20} auto-ubiquitylation does not play a major role in terminating APC/C^{Cdc20} activation in this system.

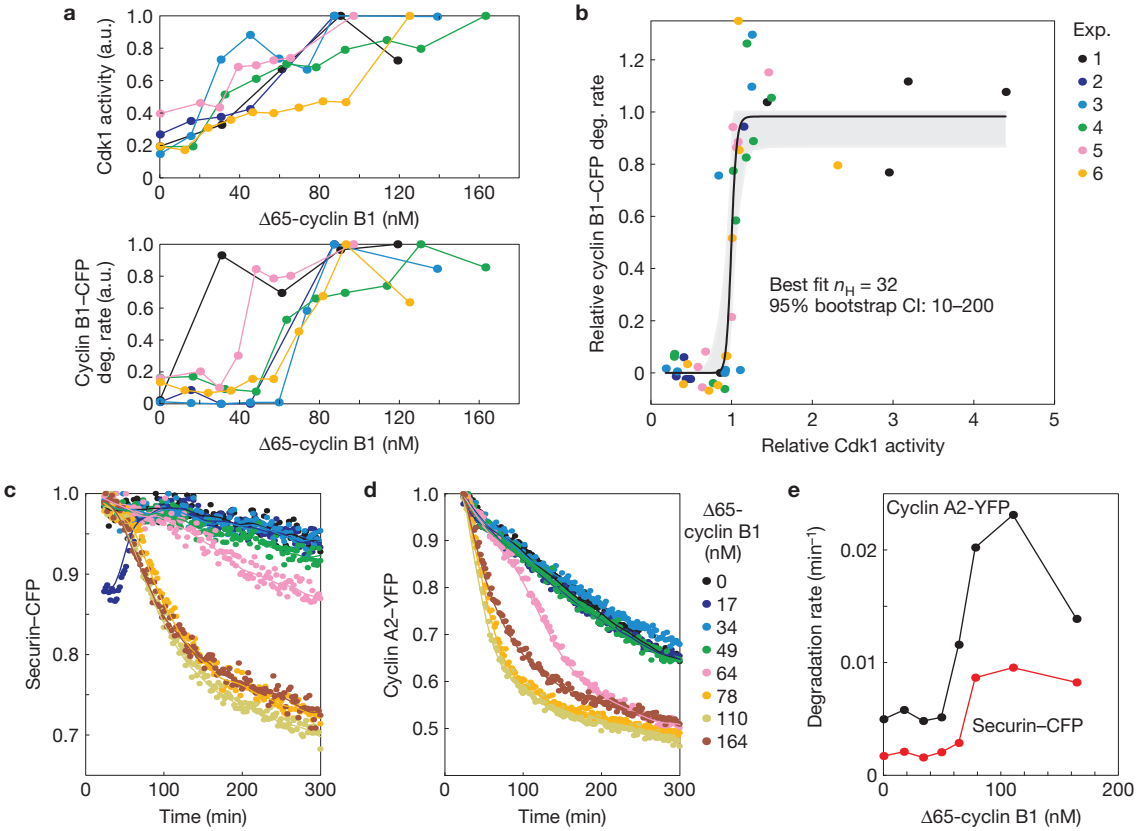

Figure 2 Ultrasensitive degradation of cyclin A2–YFP and cyclin B1–CFP. (**a**,**b**) Cyclin B1 degradation (deg.). (**a**) Cdk1 activity (top) and cyclin B1–CFP degradation (bottom) as a function of the Δ65-cyclin B1 concentration. In these experiments we used added Cdk1AF rather than added PD01166285 to make the Cdk1 response graded. (**b**) Pooled data on cyclin B1–CFP degradation versus Cdk1 activity. Data are from six independent experiments, designated by different colours. Data are scaled relative to the individual experiments' maximum degradation rates and EC_{50} values. CI, confidence interval. (**c**,**d**) Simultaneous measurement of the degradation of securin–CFP (**c**) and cyclin A2–YFP (**d**) in extracts. Extracts were treated with eight concentrations of Δ65-cyclin B1 (designated by different colours) immediately before the addition of *in vitro*-translated securin–CFP and cyclin A2–YFP, to allow for monitoring and comparison of the initiation of both APC/C substrates. For all Δ65-cyclin B1 concentrations that induced APC/C activation, the degradation of cyclin A2–YFP began about 25–40 min before the degradation of securin–CFP. (**e**) Apparent first-order rate constants for securin–CFP (red) and cyclin A2–YFP (black) degradation as a function of the Δ65-cyclin B1 concentration.

To examine the potential significance of this high ultrasensitivity, we carried out computational studies. We modelled the processes of cyclin synthesis and degradation and Cdk1 activation and inactivation (Fig. 3a) with two nonlinear ordinary differential equations (ODEs; Supplementary Note). The two-ODE model has two nullclines, and the steady state(s) of the system are found where the nullclines intersect[24] (Fig. 3b). The *Cdk1* nullcline defines the steady-state activity of Cdk1 as a function of the total concentration of cyclin present in the system, and it is S shaped owing to the bistability of the mitotic trigger (Fig. 3b, blue curve). The *Cyc* nullcline is steeply sigmoidal because of the high ultrasensitivity in the response of cyclin degradation to Cdk1 activity (Fig. 3b, red curve). Initially we chose parameters for the degradation response such that the *Cyc* nullcline intersected the middle of the *Cdk1* nullcline. The steady state at the intersection was unstable and all trajectories converged to a stable limit cycle (Fig. 3b). The result was saw-toothed oscillations in cyclin abundance and spiky oscillations in Cdk1 activity (Fig. 3c), similar to those reported from *Xenopus* extract experiments[15,25]. Note that the switch-like character of the *Cyc* nullcline made it easy to arrange for the two nullclines to intersect at a single unstable fixed point.

As the Hill exponent's assumed value decreased, the range of parameters over which a single unstable fixed point could be obtained decreased, and it was impossible to obtain oscillations when the Hill exponent was assumed to be 1; the system was always either monostable, excitable or, as shown in Fig. 3d,e, bistable. Thus, the experimentally determined shape of the *Cdk1* nullcline necessitates that the *Cyc* nullcline be sigmoidal in shape, which in turn requires that the degradation of cyclin be an ultrasensitive function of the Cdk1 activity.

To explore the relationship between the degree of ultrasensitivity and the robustness of the oscillations to parameter variation, we carried out bifurcation analyses. Figure 3f–h shows three of these, allowing the kinetic parameters for the negative feedback loop to vary for different assumed values of the Hill exponent n_H. In general, as the assumed ultrasensitivity increased, the range of parameters over which oscillations were obtained increased (Fig. 3f–h). In addition, we found that the oscillator's period and amplitude were extremely sensitive to parameter changes for low n_H, but became stable as n_H increased to the high levels seen experimentally (Fig. 3i). Thus ultrasensitive negative feedback endowed the oscillator model with robust, clock-like oscillations.

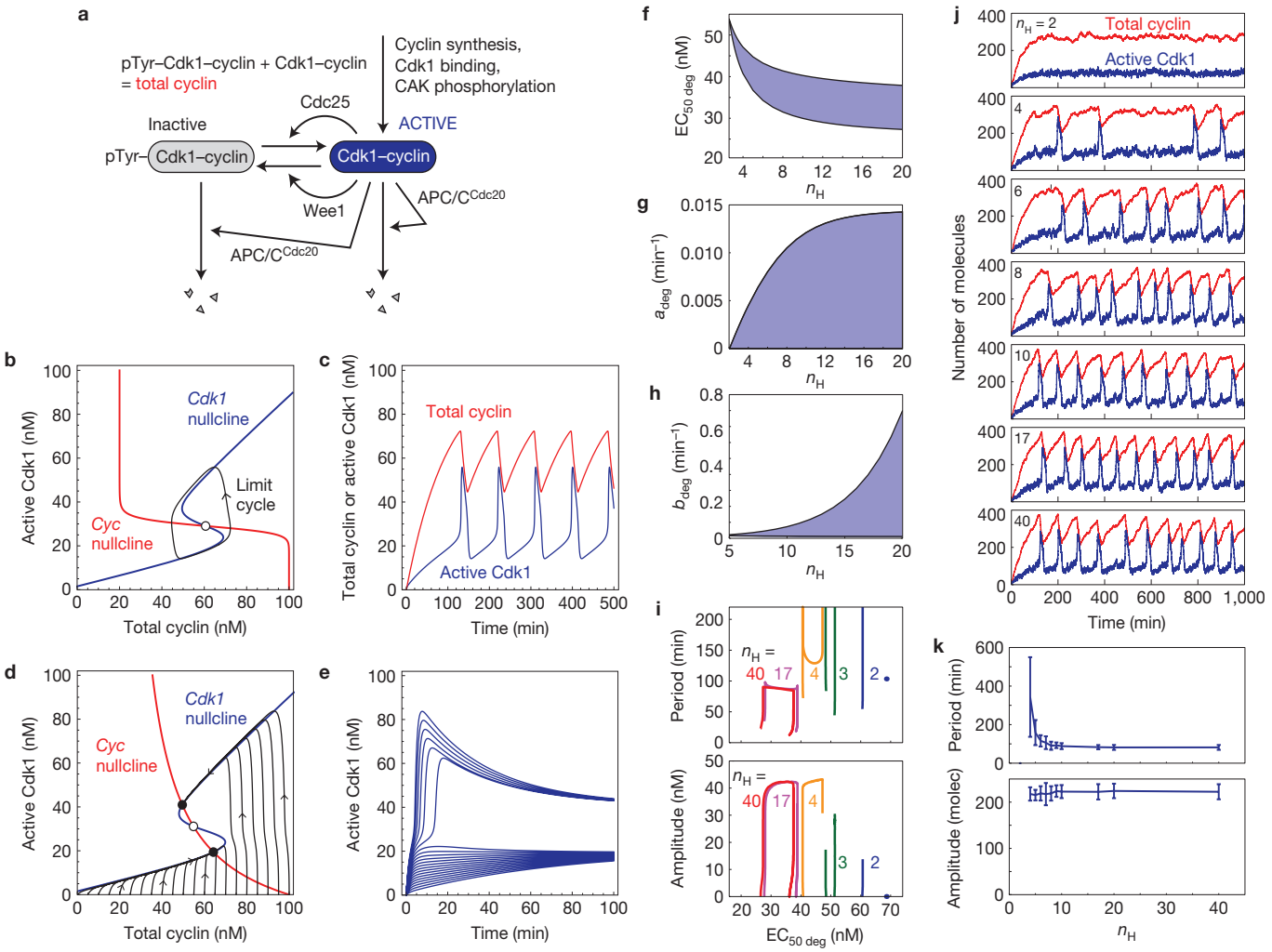

Figure 3 Ultrasensitive cyclin degradation enables limit cycle oscillations. (**a**) Schematic view of the Cdk1–APC/C^{Cdc20} system. (**b**) Phase plot of the two-ODE model. The *Cdk1* nullcline (blue) was parameterized on the basis of experimental work[17,18], and its shape agrees well with the observed hysteretic steady-state response of Cdk1 to non-degradable cyclin B1 (refs 13,14). The switch-like character of the *Cyc* nullcline (red) arises from the high Hill exponent found for the response of cyclin degradation to Cdk1 activity (Fig. 1). The two nullclines intersect at an unstable steady state (open circle), and all trajectories converge to a stable limit cycle (black). (**c**) Time course of cyclin accumulation and destruction and Cdk1 activation and inactivation in the two-ODE model. (**d**) Phase plot of the two-ODE model assuming a Hill exponent of 1 for the response of cyclin degradation to Cdk1 activity. The system is now bistable; there are two stable steady states (filled circles) and a saddle point (open circle). Sample trajectories are shown, with 15 approaching the interphase-like stable steady state (with low Cdk1 activity) and six approaching the M-phase-like stable steady state (with high Cdk1 activity). (**e**) Time course of Cdk1 activation for the trajectories shown in **d**. (**f**–**h**) Bifurcation analysis. The shaded region denotes the parameters compatible with oscillations and an unstable fixed point for the two-ODE model. (**i**) Sensitivity analysis of the period and amplitude of oscillations as a function of one bifurcation parameter, $EC_{50\ deg}$, for various assumed Hill exponents n_H. (**j**,**k**) Stochastic simulations, carried out using Gillespie's direct method, for various assumed Hill exponents n_H. (**j**) Time courses. (**k**) Variability of the period and amplitude of Cdk1 oscillations. molec, molecules. Error bars denote standard deviations.

A relatively low number of molecules in a chemical reaction can give rise to fluctuations around the deterministic dynamics, which can result in variation in both the period and amplitude of oscillations. The total number of cyclin and active Cdk1 molecules present in a *Xenopus* egg is not actually low ($\sim 10^{10}$ molecules per egg). However, it is possible that critical subpopulations of the Cdk1 complexes, such as those associated with the centrosome, may be small enough in number that stochastic fluctuations become significant. Moreover, the same basic circuit functions in small cells (for example yeasts). We therefore asked whether ultrasensitivity in the negative loop affected the system's robustness to stochastic fluctuations. We converted the two-ODE model into the master equation framework and carried out numerical simulations. Rate constants from the ODE model were converted such that the peak numbers of cyclin and active Cdk1 molecules were small enough to make the stochastic variations in cyclin and active Cdk1 readily apparent. As shown in Fig. 3i,j, ultrasensitive negative feedback made the period of the oscillations more resistant to intrinsic stochastic noise.

One longstanding hypothesis for how the order of cell cycle events is established is that early events require relatively low levels of Cdk1 activity, whereas late events require higher levels[26,27]. This hypothesis was originally inspired by studies in *Schizosaccharomyces pombe*, where a single cyclin–Cdk complex is primarily responsible for both S phase and M phase[26]. In other organisms, where different cyclin–Cdks

regulate different cell cycle phases, this hypothesis can be modified to apply to the ordering of events within a phase. For example, early mitotic events, such as nuclear envelope breakdown, might require low levels of cyclin B1–Cdk1 activity, whereas late mitotic events such as APC/C^{Cdc20} activation might require high levels. This could keep Cdk1 and APC/C^{Cdc20} activities out of phase with each other, and help ensure robust oscillations. However, previous experimental tests of this hypothesis have yielded mixed results. Clb2 titration experiments in *S. cerevisiae* support the differential threshold model[28], whereas live cell imaging studies in human cell lines indicate that the amount of Cdk1 activity required for APC/C^{Cdc20} activation is lower, not higher, than the amount required for nuclear envelope breakdown[29].

Our modelling studies bear on this issue. Given the experimentally determined shapes of the Cdc25 and Wee1 response functions, only a limited range of EC_{50} values for APC/C^{Cdc20} activation are compatible with oscillations, and these values are similar to the measured values for the (early) Cdc25 and Wee1 responses (Fig. 4a).

We therefore set out to directly test whether securin–CFP degradation requires a relatively high level of Cdk1 activity, as predicted by the differential threshold hypothesis, or a low level, as predicted by the two-ODE model. To this end we simultaneously assessed the stimulus–response relationships for securin–CFP degradation, Wee1 Thr 150 phosphorylation and Cdc25 hyperphosphorylation (two early mitotic events), and Cdc27 (APC3) phosphorylation (a late mitotic event)[30,31]. The concentration of Δ65-cyclin B1 and the level of Cdk1 activation required to half-maximally activate securin–CFP degradation were found to be comparable to those required for half-maximal Cdc25 and Wee1 phosphorylation (Fig. 4b,c). Thus, although differential thresholds are important for ordering some cell cycle events[26,27,32,33], a different strategy must be employed in the *Xenopus* embryonic cell cycle. Interestingly, Cdc27 phosphorylation did require higher levels of Cdk1 activity than did the other mitotic events, and there was little Cdc27 phosphorylation at concentrations of Δ65-cyclin B1 that were just sufficient to induce maximal APC/C^{Cdc20} activation (Fig. 4b,c). This indicates that there is not a simple relationship between the overall phosphorylation of this APC/C subunit and APC/C^{Cdc20} activity.

As mentioned above, time delays in negative feedback loops tend to promote oscillations[5–7] and, in the case of the *Xenopus* embryonic cell cycle where a differential threshold strategy is not applicable, such time delays could also help ensure that Cdk1-dependent mitotic events are completed before Cdk1 inactivation and mitotic exit take place. In most cells, the spindle assembly checkpoint provides a time delay in the degradation of the critical substrates cyclin B1 and securin (but not cyclin A, Nek2A or HoxC10; ref. 34). However, in *Xenopus* eggs and embryos the checkpoint is not operative[21]. We therefore asked if an intrinsic time delay was built into the Cdk1–APC/C^{Cdc20} loop and, if so, which step in the loop (APC/C activation or cyclin degradation) generated the delay.

The total time lag between Cdk1 activation and securin–CFP degradation was assessed by simultaneously adding both Δ65-cyclin B1 and securin–CFP to an interphase extract, measuring the time course of Cdk1 activation and securin–CFP degradation, and asking by how much the latter lagged behind the former (Fig. 5b,c). A mitotic concentration of Δ65-cyclin B1 (89 nM) was used and the inhibitor PD0166285 was included, which minimized the time needed for Cdk1 activation to plateau (Fig. 5c). To obtain a quantitative estimate of the apparent first-order rate constant for securin–CFP degradation, the securin–CFP fluorescence data were smoothed using the Gaussian kernel technique (Fig. 5b, solid line), degradation rates were calculated by numerical differentiation, and rate constants were calculated.

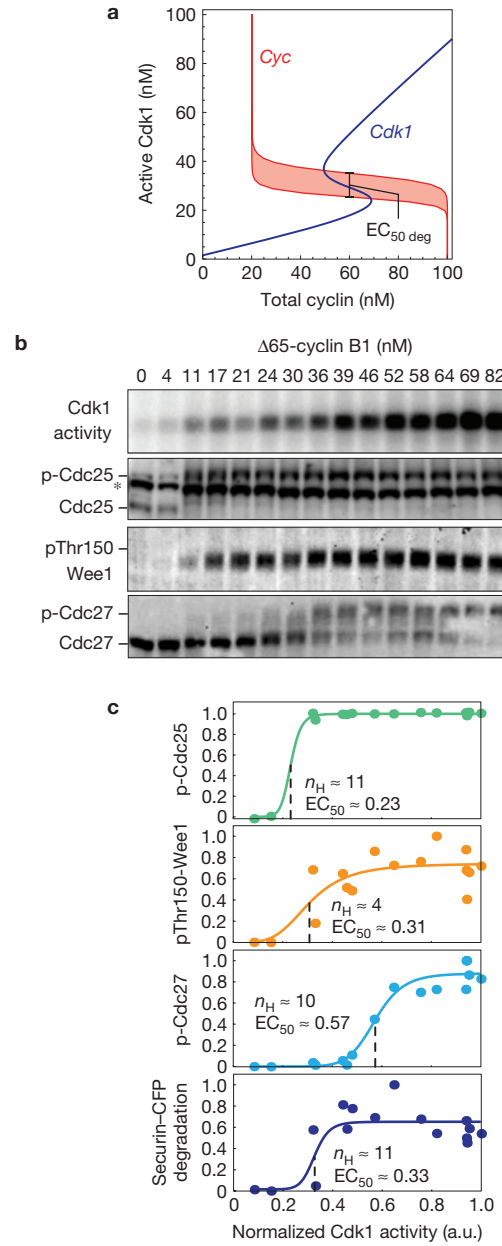

Figure 4 The EC_{50} values for APC/C^{Cdc20} activation, Cdc25 phosphorylation and Wee1 phosphorylation are similar. (**a**) Nullclines for the two-ODE Cdk1–APC/C^{Cdc20} model showing the range of cyclin degradation EC_{50} values over which the model yields unique limit cycles. At an EC_{50} value of approximately 28 nM, oscillations arise through a supercritical Hopf bifurcation. At $EC_{50} \approx 38$ nM, the system goes through a subcritical Hopf bifurcation and oscillations begin to disappear. Thus, oscillations are possible only for a tight range of EC_{50} values similar to those assumed for Cdc25 (35 nM) and Wee1 (30 nM). (**b**) Steady-state stimulus–response studies for Cdk1 activation, Cdc25 hyperphosphorylation, Wee1 Thr 150 phosphorylation and Cdc27 phosphorylation. The top panel is an autoradiogram of a histone H1 kinase assay. The other three panels are immunoblots. The band designated by an asterisk on the Cdc25 blot is a background band. Full gel scans are shown in Supplementary Fig. S3. (**c**) Steady-state dose–response curves.

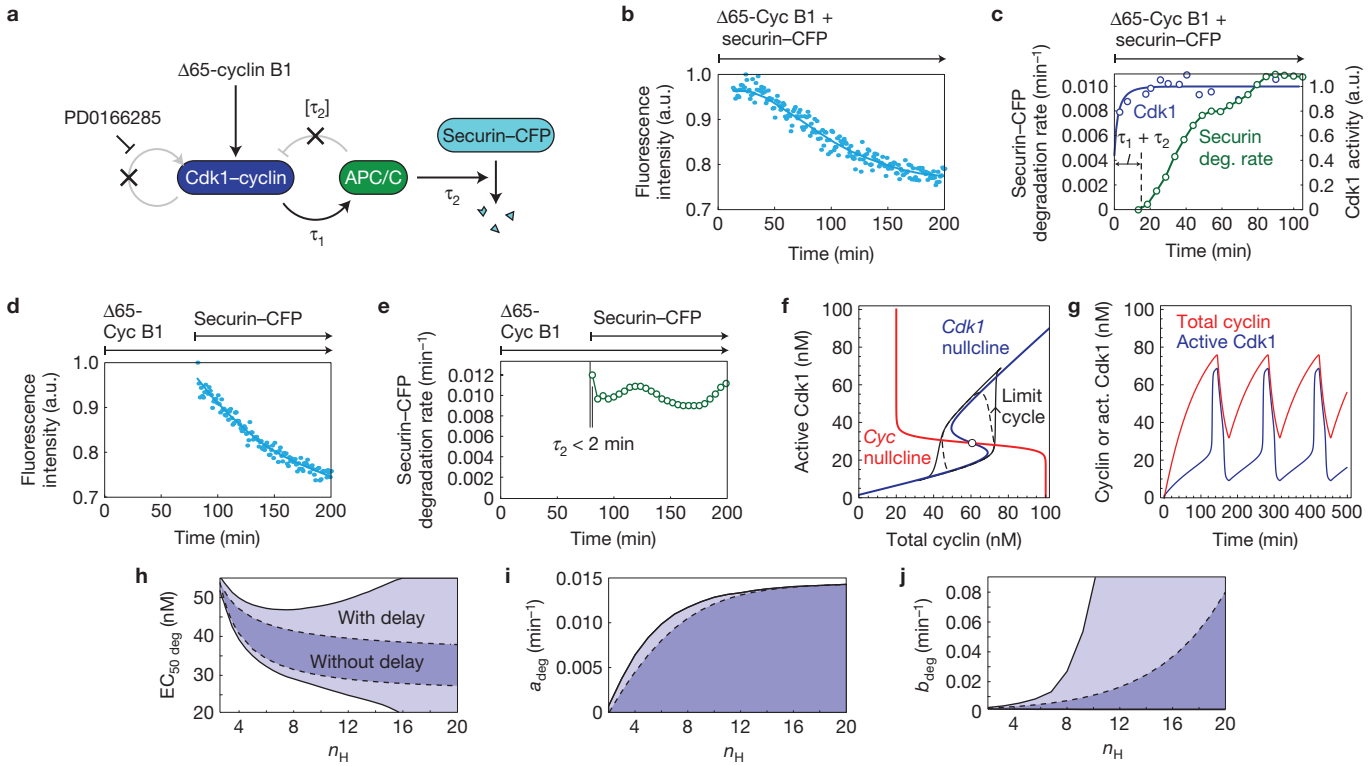

Figure 5 Time lags in the *Xenopus* embryonic cell cycle oscillator's negative feedback loop. (**a**) Schematic view of the experimental design. Interphase *Xenopus* egg extracts were prepared. A non-degradable cyclin protein (Δ65-cyclin B1) was added to activate Cdk1 and APC/C^{Cdc20}. PD0166285, an inhibitor of Wee1A and Myt1, was included to enable a graded range of Cdk1 activities to be obtained. (**b**,**c**) Time lag between Cdk1 activation and securin–CFP degradation (deg.). These data imply that $\tau_1 + \tau_2 \approx 15$ min. (**d**,**e**) Time lag between APC/C^{Cdc20} activation and securin–CFP degradation. The upper bound for τ_2 is estimated to be 2 min. See also Supplementary Fig. S2. (**f**–**j**) Computational analysis. (**f**) Phase plot of the two-DDE model, assuming $\tau = 15$ min. The two nullclines are the same as those shown in Fig. 3b. All trajectories converge to a stable limit cycle (black). The limit cycle for the two-ODE model (that is, $\tau = 0$) is shown as a dashed curve for comparison. (**g**) Time course of cyclin accumulation and destruction and Cdk1 activation and inactivation in the two-DDE model (act., active). (**h**–**j**) Bifurcation analysis. The light blue shading denotes the parameters compatible with oscillations for the two-DDE model, but not for the two-ODE model. The dark blue shading denotes parameters compatible with oscillations for both the DDE and ODE models.

As shown in Fig. 5b, securin–CFP degradation was initially slow and then accelerated, with the time lag between Cdk1 activation and securin–CFP degradation estimated to be ~15 min (Fig. 5c). This value agrees well with the time lags seen in previous studies of cyclin degradation in *Xenopus* extracts supplemented with active starfish Cdk1–cyclin B (ref. 16). The observed delay includes both the time between Cdk1 activation and APC/C^{Cdc20} activation (τ_1) and the time between APC/C^{Cdc20} activation and securin–CFP degradation (τ_2). Lower concentrations of Δ65-cyclin B1 yielded longer time lags (Supplementary Fig. S4).

To determine whether a time lag between APC/C activation and the onset of securin–CFP destruction (τ_2) contributed to the observed delay, the experiment was repeated with the securin–CFP added 80 min after Δ65-cyclin B1, at a time when APC/C^{Cdc20} activity should be close to its steady-state level. We then asked how quickly the securin–CFP fluorescence began to decrease. As shown in Fig. 4e, the measured fluorescence began dropping as soon as the securin–CFP was added to the extract. The apparent rate constant was maximal by the first times, and τ_2 was estimated to be no greater than 2 min (Fig. 5e). Similar results were obtained with other Δ65-cyclin B1 concentrations; the time lag between addition of securin–CFP and its degradation was always too short to measure.

Taken together, these experiments demonstrate that there is a substantial (~15 min) time delay in the Cdk1-to-APC/C^{Cdc20} leg of the negative feedback loop, and no detectable (<2 min) delay in the APC/C^{Cdc20}-to-Cdk1 leg.

To explore the potential significance of the time lag, we modified the two-ODE model to include an explicit time delay between Cdk1 activation and cyclin degradation, yielding a pair of delay differential equations (DDEs; Supplementary Note). With all other parameters held unchanged, a 15 min time delay slowed the period and increased the amplitude of the oscillations (Fig. 5f,g), without markedly affecting the qualitative character of the oscillations (sawtooth oscillations in cyclin, spike-like oscillations in active Cdk1). The time delay also increased the robustness of the oscillations to parameter variation (Fig. 5h–j). Nevertheless, even with the time delay, ultrasensitivity in the degradation response was still required to obtain oscillations.

Alternatively, we modelled the time lag as arising from a multistep mechanism for the activation of APC/C^{Cdc20} by Cdk1 (Supplementary Note). Again, we found that time lags contributed to the robustness of oscillations (Supplementary Fig. S5).

In summary, we have quantitatively characterized the negative feedback loop on which the embryonic cell cycle oscillator is built. We found that Cdk1-induced degradation of securin, cyclin A2 and cyclin

B1 is extremely switch-like, with steady-state responses equivalent to those of a cooperative process with a Hill exponent of at least 17 (Figs 1 and 2). In addition, there is a substantial delay (∼15 min) between Cdk1 activation and APC/C^{Cdc20} activation (Fig. 5). Thus, even when the bistable trigger is eliminated from consideration, the core negative feedback loop functions as a time-delayed digital switch. Early theoretical studies of generic oscillator circuits established that both time delays and ultrasensitivity can help keep a negative feedback loop from settling into a stable steady state[1,4,5]. The present work shows that both of these design features are in fact present, and present to a remarkable degree, in the *Xenopus* embryonic cell cycle oscillator. ODE and DDE models of the circuit indicate that the ultrasensitivity and time delays endow the circuit with a clock-like period, a constant amplitude and robustness with respect to fluctuations in component concentrations and changes in kinetic parameters (Figs 3, 5 and Supplementary Fig. S5).

Although the details of the APC/C^{Cdc20} activation mechanism are incompletely understood, some mechanisms that can generate ultrasensitivity also generate substantial time lags. For example, the observed steady-state and dynamic behaviours of the negative feedback loop are consistent with a multistep phosphorylation activation mechanism (Supplementary Fig. S5), with the nominal number of steps being approximately 25–30. If the phosphatase that reverses these phosphorylations is regulated by Cdk1, as is the case for PP2A-B55δ (ref. 19), this regulation could also contribute to the ultrasensitivity and time lag. In any case, both high Hill exponents and time lags seem to be commonplace in the cell cycle oscillator circuit[16–18,35,36].

In summary, the present work shows that the negative feedback loop on which the *Xenopus* embryonic cell cycle oscillator is built functions as a time-delayed, ultrasensitive switch. Given the diversity of biological oscillations, it will be of great interest to see whether this proves to be a recurring design strategy for biological clocks. □

METHODS

Methods and any associated references are available in the online version of the paper.

Note: Supplementary Information is available in the online version of the paper

ACKNOWLEDGEMENTS

We thank J. Chang and A. Poon for help obtaining purified Δ65-cyclin B1 and Cdk1AF proteins, S. Santos and J. Pomerening for cyclin B1–CFP and cyclin A2–YFP constructs, T. Tsai for sharing his findings on the effects of PD0166285 on *Xenopus* Wee1A and Myt1, R. Driscoll from the Cimprich laboratory for advice on freezing extracts, and G. Anderson, J. Chang, A. Moskaleva, T. Tsai and the rest of the Ferrell laboratory for scientific discussions and editorial suggestions. We also thank Pfizer for providing PD0166285. Q.Y. is an HHMI Fellow of the Damon Runyon Cancer Research Foundation (DRG-2081-11). This work was supported by the National Institutes of Health grant GM046383.

AUTHOR CONTRIBUTIONS

Q.Y. carried out experiments and calculations, analysed data and helped write the paper. J.E.F. carried out calculations, analysed data and helped write the paper.

COMPETING FINANCIAL INTERESTS

The authors declare no competing financial interests.

Published online at www.nature.com/doifinder/10.1038/ncb2737
Reprints and permissions information is available online at www.nature.com/reprints

1. Goldbeter, A. *Biochemical Oscillations and Cellular Rhythms: The Molecular Bases of Periodic and Chaotic Behaviour* (Cambridge Univ. Press, 1996).
2. Thomas, R. On the relation between the logical structure of systems and their ability to generate multiple steady states or sustained oscillations. *Springer Ser. Synergetics* **9,** 180–193 (1981).
3. Becskei, A. & Serrano, L. Engineering stability in gene networks by autoregulation. *Nature* **405,** 590–593 (2000).
4. Griffith, J. S. Mathematics of cellular control processes. I. Negative feedback to one gene. *J. Theor. Biol.* **20,** 202–208 (1968).
5. Tyson, J. J. & Othmer, H. G. The dynamics of feedback control circuits in biochemical pathways. *Prog. Theor. Biol.* **5,** 1–62 (1978).
6. Novak, B. & Tyson, J. J. Design principles of biochemical oscillators. *Nat. Rev. Mol. Cell Biol.* **9,** 981–991 (2008).
7. Stricker, J., Cookson, S., Bennett, M., Tsimring, L. & Hasty, J. A fast, robust, and tunable synthetic gene oscillator. *Nature* **456,** 516–519 (2008).
8. Tsai, T. Y. *et al.* Robust, tunable biological oscillations from interlinked positive and negative feedback loops. *Science* **321,** 126–129 (2008).
9. Hara, K., Tydeman, P. & Kirschner, M. A cytoplasmic clock with the same period as the division cycle in *Xenopus* eggs. *Proc. Natl Acad. Sci. USA* **77,** 462–466 (1980).
10. Murray, A. W. & Kirschner, M. W. Dominoes and clocks: the union of two views of the cell cycle. *Science* **246,** 614–621 (1989).
11. Pines, J. Cubism and the cell cycle: the many faces of the APC/C. *Nat. Rev. Mol. Cell Biol.* **12,** 427–438 (2011).
12. King, R. W. *et al.* A 20S complex containing CDC27 and CDC16 catalyzes the mitosis-specific conjugation of ubiquitin to cyclin B. *Cell* **81,** 279–288 (1995).
13. Sha, W. *et al.* Hysteresis drives cell-cycle transitions in *Xenopus laevis* egg extracts. *Proc. Natl Acad. Sci. USA* **100,** 975–980 (2003).
14. Pomerening, J. R., Sontag, E. D. & Ferrell, J. E. Jr Building a cell cycle oscillator: hysteresis and bistability in the activation of Cdc2. *Nat. Cell Biol.* **5,** 346–351 (2003).
15. Pomerening, J. R., Kim, S. Y. & Ferrell, J. E. Jr Systems-level dissection of the cell-cycle oscillator: bypassing positive feedback produces damped oscillations. *Cell* **122,** 565–578 (2005).
16. Felix, M. A., Labbe, J. C., Doree, M., Hunt, T. & Karsenti, E. Triggering of cyclin degradation in interphase extracts of amphibian eggs by cdc2 kinase. *Nature* **346,** 379–382 (1990).
17. Kim, S. Y. & Ferrell, J. E. Jr Substrate competition as a source of ultrasensitivity in the inactivation of Wee1. *Cell* **128,** 1133–1145 (2007).
18. Trunnell, N. B., Poon, A. C., Kim, S. Y. & Ferrell, J. E. Jr Ultrasensitivity in the regulation of Cdc25C by Cdk1. *Mol. Cell* **41,** 263–274 (2011).
19. Mochida, S., Ikeo, S., Gannon, J. & Hunt, T. Regulated activity of PP2A-B55 delta is crucial for controlling entry into and exit from mitosis in *Xenopus* egg extracts. *EMBO J.* **28,** 2777–2785 (2009).
20. Izawa, D. & Pines, J. How APC/C-Cdc20 changes its substrate specificity in mitosis. *Nat. Cell Biol.* **13,** 223–233 (2011).
21. Minshull, J., Sun, H., Tonks, N. K. & Murray, A. W. A MAP kinase-dependent spindle assembly checkpoint in *Xenopus* egg extracts. *Cell* **79,** 475–486 (1994).
22. Minshull, J., Golsteyn, R., Hill, C. S. & Hunt, T. The A- and B-type cyclin associated cdc2 kinases in *Xenopus* turn on and off at different times in the cell cycle. *EMBO J.* **9,** 2865–2875 (1990).
23. Foe, I. T. *et al.* Ubiquitination of Cdc20 by the APC occurs through an intramolecular mechanism. *Curr. Biol.* **21,** 1870–1877 (2011).
24. Strogatz, S. H. *Nonlinear Dynamics and Chaos: With Applications to Physics, Biology, Chemistry, and Engineering* (Westview Press, 1994).
25. Murray, A. W. & Kirschner, M. W. Cyclin synthesis drives the early embryonic cell cycle. *Nature* **339,** 275–280 (1989).
26. Stern, B. & Nurse, P. A quantitative model for the cdc2 control of S phase and mitosis in fission yeast. *Trends Gene.* **12,** 345–350 (1996).
27. Coudreuse, D. & Nurse, P. Driving the cell cycle with a minimal CDK control network. *Nature* **468,** 1074–1079 (2010).
28. Oikonomou, C. & Cross, F. R. Rising cyclin-CDK levels order cell cycle events. *PLoS One* **6,** e20788 (2011).
29. Gavet, O. & Pines, J. Progressive activation of CyclinB1–Cdk1 coordinates entry to mitosis. *Dev. Cell* **18,** 533–543 (2010).
30. Georgi, A. B., Stukenberg, P. T. & Kirschner, M. W. Timing of events in mitosis. *Curr. Biol.* **12,** 105–114 (2002).
31. Kim, S. Y., Song, E. J., Lee, K. J. & Ferrell, J. E. Jr Multisite M-phase phosphorylation of *Xenopus* Wee1A. *Mol. Cell Biol.* **25,** 10580–10590 (2005).
32. Skotheim, J. M., Di Talia, S., Siggia, E. D. & Cross, F. R. Positive feedback of G1 cyclins ensures coherent cell cycle entry. *Nature* **454,** 291–296 (2008).
33. Doncic, A., Falleur-Fettig, M. & Skotheim, J. M. Distinct interactions select and maintain a specific cell fate. *Mol. Cell* **43,** 528–539 (2011).
34. Kimata, Y., Baxter, J. E., Fry, A. M. & Yamano, H. A role for the Fizzy/Cdc20 family of proteins in activation of the APC/C distinct from substrate recruitment. *Mol. Cell* **32,** 576–583 (2008).
35. Solomon, M. J., Glotzer, M., Lee, T. H., Philippe, M. & Kirschner, M. W. Cyclin activation of $p34^{cdc2}$. *Cell* **63,** 1013–1024 (1990).
36. Nash, P. *et al.* Multi-site phosphorylation of a CDK inhibitor sets a threshold for the onset of S-phase. *Nature* **414,** 514–521 (2001).

DOI: 10.1038/ncb2737

METHODS

Preparation of *Xenopus* egg extracts. Undiluted interphase egg extracts treated with 100 μg ml^{-1} cycloheximide were prepared as described[37,38], except that eggs were activated with calcium ionophore A23187 (200 ng μl^{-1}) rather than electric shock. In these extracts, endogenous cyclin B1 has been degraded and Cdk1 is inactive. Some experiments used frozen stocks of interphase extracts, with no noticeable decrease in Cdk1 and APC activities. The freezing procedure is described as follows. Freshly prepared extracts[37,38] were mixed with 80% glycerol to give a final concentration of 3%, then fast-frozen in 50 μl aliquots in liquid nitrogen, and stored at −80 °C refrigerator for up to 6 months.

To drive the interphase extracts into a series of intermediate Cdk1 activity states, an inhibitor of Wee1 and Myt1 (PD0166285) was included (500 nM), and various concentrations of purified recombinant Δ65-cyclin B1 ranging from 0 to 200 nM (to interrupt the negative feedback and to drive Cdk1 activation) were added. In a few experiments (Fig. 2 and data not shown) we used Cdk1AF (200 nM) rather than PD0166285 to make the Cdk1 response graded. The Δ65-cyclin B1-supplemented extracts were incubated at room temperature for 90–120 min until they reached steady state and were then taken for simultaneous measurements of both Cdk1 and APC/C activities. Generally we did not add sperm chromatin to the extracts.

H1 kinase assay and automatic gel image analysis. H1 kinase assays were carried out as described[38]. ^{32}P-labelled histone was detected using a PhosphorImager. To allow for consistent quantification, gel images were analysed by an automatic gel image processing program written in MATLAB, on the basis of a marker-controlled watershed algorithm. Assays were typically carried out in duplicate or triplicate.

Real-time fluorescence assay for APC/C^{Cdc20} substrate degradation in *Xenopus* extracts. Fluorescent APC/C substrate proteins have been used to monitor APC/C^{Cdc20} and APC/C^{Cdh1} activities in real time in mammalian cell lines[39]. Here we developed a similar real-time assay for *Xenopus* egg extracts. We constructed complementary DNAs for various fluorescent (YFP-, CFP-, tdimer2-, or BODIPY-tagged) APC/C substrates and expressed them *in vitro* in a wheat-germ system (TNT SP6 High Yield Protein Expression, Promega). In general, the CFP-tagged substrates showed the best signal-to-noise values, well above the background of the extracts' autofluorescence.

A small amount (0.5–1 μl out of the 50 μl reaction) of the *in vitro*-translated securin–CFP, cyclin B1–CFP and/or cyclin A2–YFP was added to each (15–20 μl) of the extracts, with varying steady-state levels of Cdk1 and APC/C^{Cdc20} activity. Extracts were immediately loaded in a small volume 384-well black plate (Greiner) and the degradation of securin–CFP, cyclin B1–CFP and/or cyclin A2–YFP was monitored in real time using a fluorescence microplate reader (FLEXstation II 384). Duplicates or triplicates were typically used.

Control experiments established that photobleaching was insignificant (Supplementary Fig. S1).

Bootstrapping techniques. To avoid one experiment dominating the curve fitting, we used a bootstrap resampling method to calculate 95% confidence intervals for the pooled data shown in Figs 1 and 2. We created 1,000 samples by sampling with replacement from each pooled dataset. Histograms of fitting parameters from 1,000 bootstrap samples corresponding to Fig. 1f indicated significant ultrasensitivity in the response of APC/C^{Cdc20} to Cdk1.

37. Smythe, C. & Newport, J. W. Systems for the study of nuclear assembly, DNA replication, and nuclear breakdown in *Xenopus laevis* egg extracts. *Meth. Cell Biol.* **35,** 449–468 (1991).
38. Murray, A. W. Cell cycle extracts. *Meth. Cell Biol.* **36,** 581–605 (1991).
39. Hagting, A. *et al.* Human securin proteolysis is controlled by the spindle checkpoint and reveals when the APC/C switches from activation by Cdc20 to Cdh1. *J. Cell Biol.* **157,** 1125–1137 (2002).

DOI: 10.1038/ncb2737

nature cell biology

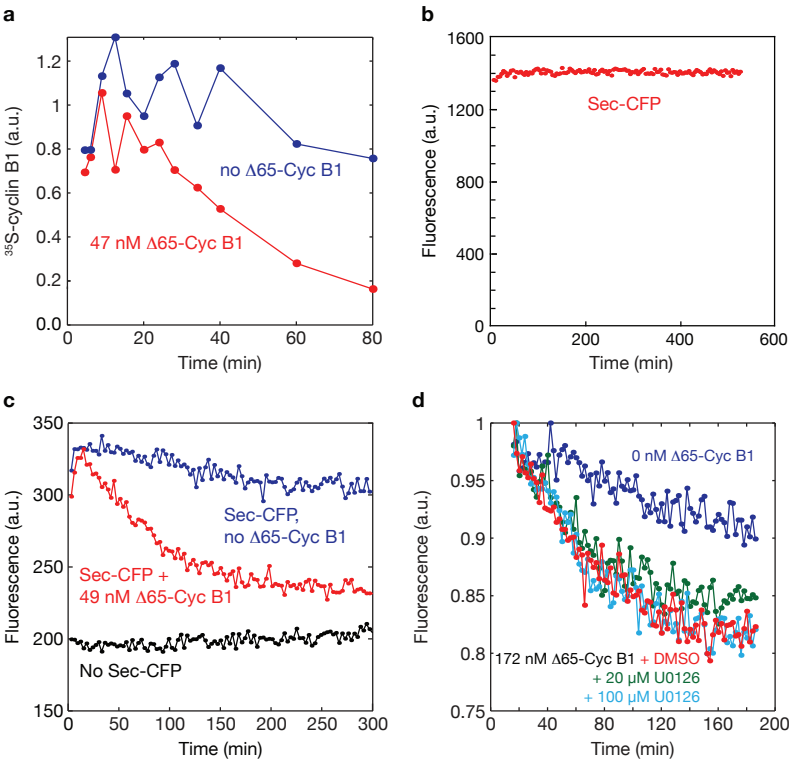

Figure S1 Control experiments for the securin and cyclin degradation assays. Related to Fig 1. **a**, Degradation of ^{35}S-labeled, in vitro-translated cyclin B1, in an interphase extract (blue) and a mitotic extract (red). **b**, Stability of in vitro translated securin-CFP to photobleaching. The stability of cyclin B1-CFP and cyclin A2-YFP was similarly high (not shown). **c**, Degradation of securin-CFP in an interphase extract (blue) and a mitotic extract (red), and autofluorescence of the interphase extract. **d**, Degradation of securin-CFP in the absence and presence of the MEK inhibitor U0126.

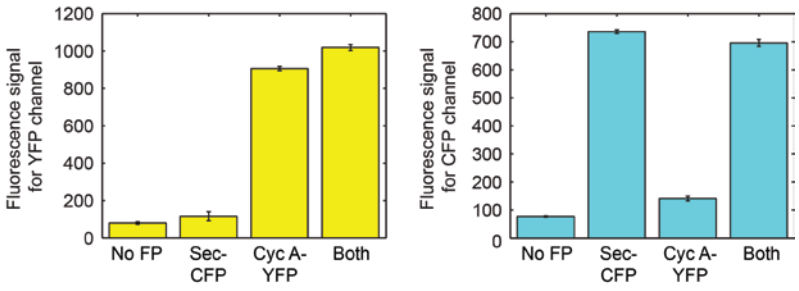

Figure S2 Minimal cross-talk in the two color securin-CFP and cyclin A1-YFP degradation assay. Related to Fig. 2. Interphase extracts were supplemented with securin-CFP, cyclin A1-YFP, or both proteins. Fluorescence emission data over the course of 410 min are expressed as means ± S.D.

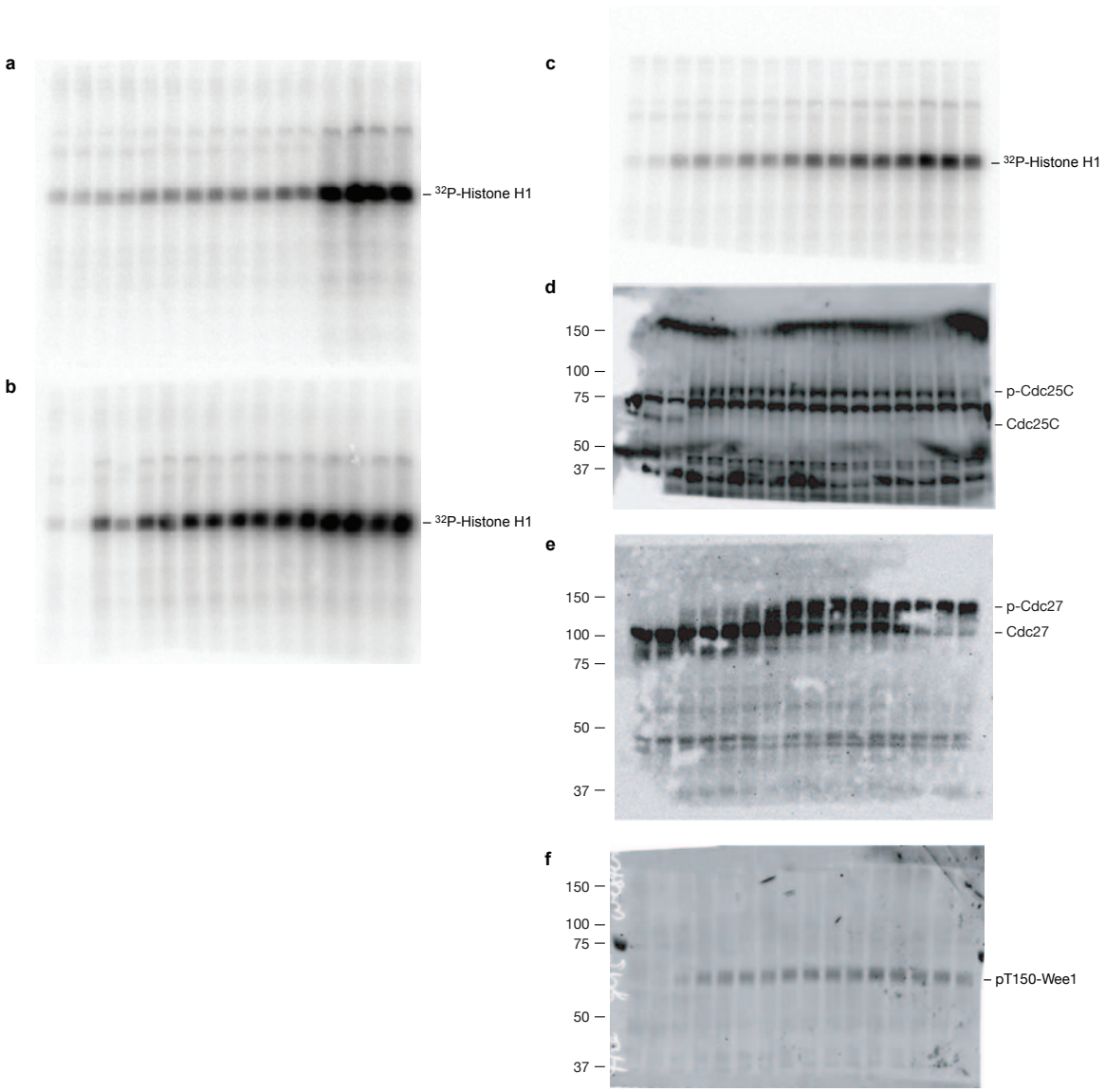

Figure S3 Full scans of the gels/blots shown in Figs. 1b and 4b. **a**, Cdk1 activity, based on histone H1 phosphorylation, in the absence of PD0166285. Related to Fig 1b. **b**, Cdk1 activity, based on histone H1 phosphorylation, in the presence of PD0166285. Related to Fig 1b. **c**, Cdk1 activity, based on histone H1 phosphorylation. Related to Fig 4b. **d**, Cdc25C hyperphosphorylation, based on Cdc25C immunoblotting. Related to Fig 4b. **e**, Wee1A T150 phosphorylation, based on pT150-Wee1 immunoblotting. Related to Fig 4b. **f**, Cdc27 hyperphosphorylation, based on Cdc27 immunoblotting. Related to Fig 4b.

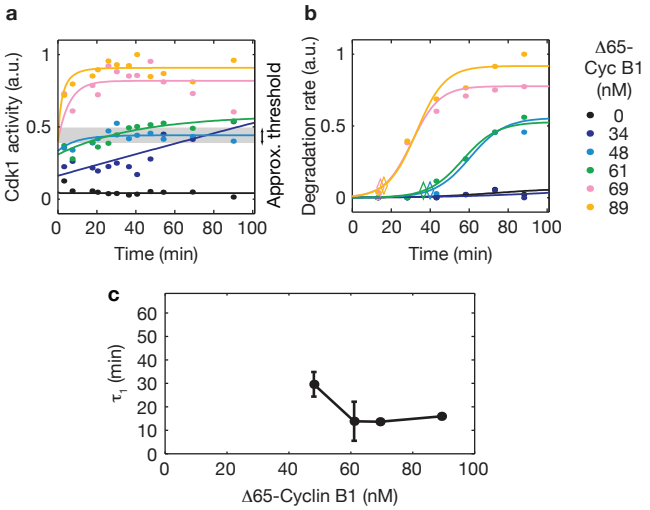

Figure S4 Additional data on the time lag between Cdk1 activation and securin degradation. Related to Fig. 5. **a**, Cdk1 activity as a function of time, for various concentrations of added Δ65-cyclin B1. Data were fitted by a model assuming that Cdk1 is activated by Δ65-cyclin-B1 through mass-action kinetics, as should be the case when positive feedback has been successfully interrupted by inhibition of Wee1A and Myt1. **b**, Degradation rates as a function of time. Data were fitted to logistic curves. The places where the fitted curves had maximal second derivatives are designated by diamonds. Note that 48 nM cyclin Δ65-cyclin B1 was sufficient to induce degradation of securin-CFP, but 34 nM was not. Therefore the threshold level of Cdk1 activity needed for degradation, in this experiment, was ~0.4-0.5 arbitrary units. **c**, Inferred lag times, calculated based on the times when Cdk1 activity reached the threshold for APC activation (**a**) and the times when the securin-CFP degradation rates began to increase (**b**).

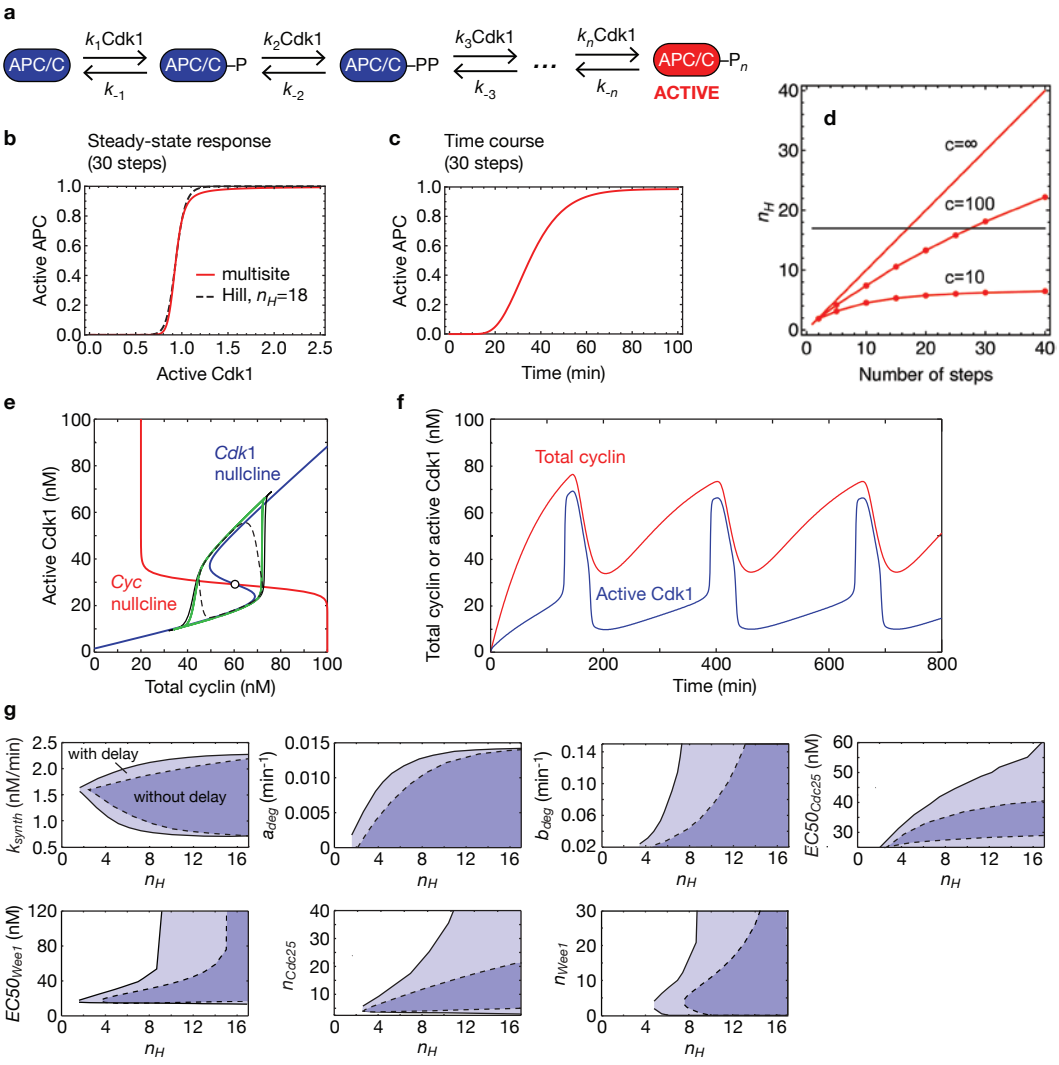

Figure S5 Multisite phosphorylation as a mechanism for generating ultrasensitivity and a time lag in the APC/C^{Cdc20} response. Related to Fig. 5. **a**, Schematic depiction of the activation of APC/C^{Cdc20} by multisite phosphorylation. We assume that a simple multistep phosphorylation reaction leads to the production of active APC/C^{Cdc20}. **b, c**, Calculated steady-state (b) and dynamical (c) responses to a constant level of Cdk1 activity. For all of the steps except the last, we assumed that $k_i/k_{-i}=1$. For the final (nth) step we assume that $k_n/k_{-n}=100$. **d**, Effective Hill exponents for other assumed ratios of k_n/k_{-n}. The effective Hill exponent was calculated from the steady-state response curves using the formula $n_H=\frac{Log_{10}[81]}{Log_{10}[EC90/EC10]}$. The horizontal line corresponds to $n_H=17$, the value inferred for APC/C^{Cdc20}-mediated securin-CFP degradation (Fig. 1). **e,** Phase plot for the oscillator model. The stable limit cycle for the 32-ODE model is shown in green. The limit cycles for the 2-ODE model and the DDE model are shown in dashed black and solid black, respectively. **f,** Time course of cyclin and Cdk1 oscillations for the 32-ODE model. **g**, Bifurcation diagrams for an ODE oscillator model that generates realistic (15 min) time lags through multisite phosphorylation. The dark blue region shows the parameters that generate oscillations for the 2-ODE model, with the region's boundary (dashed line) taken from the position of the Hopf bifurcation. The light blue region shows the additional region compatible with oscillations for the 32-ODE multisite phosphorylation oscillator model.